Journal of Sound and Vibration (1997) **207**(5), 731–742

VIBRATION OF MULTI-SPAN TIMOSHENKO BEAMS TO A MOVING FORCE

R.-T. WANG

Department of Engineering Science, National Cheng Kung University, Tainan, Taiwan, Republic of China

(*Received* 22 *January* 1996, *and in final form* 6 *June* 1997)

A method of modal analysis is proposed in this paper to investigate the forced vibration of multi-span Timoshenko beams. The ratio of the radius of gyration of the cross-section to one span length is defined as a parameter r. The effect of r on the first modal frequency of a beam is studied. A concentrated force traversing on the beam is used as an example. The effects of span number, rotatory inertia and shear deformation on the maximum moment, the maximum deflection and the critical velocity of a beam are examined. The results are compared with those of a multi-span Bernoulli–Euler beam.

1. INTRODUCTION

Numerous studies concerning the dynamics of one-span beams to moving loads have been reported in the literature [1, 2]. The responses of these beams are functions of both time and velocity. Every beam deforms seriously at its critical velocity [3]. In most cases, both the maximum deflection and the maximum moment of a beam induced by a moving load are greater than those induced by the same static load. These response phenomena and the critical velocity make the problem of moving loads an interesting topic in structural dynamics.

Usually, the beam structures on which loads move are regularly supported. This kind of beam is called a multi-span beam. A typical example of a multi-span beam is a continuous guideway. The critical velocity of a continuous guideway is the lowest phase velocity of the bending wave in the structure [4]. The dynamic responses of multi-span Bernoulli–Euler beams to moving loads were studied by Wang [5]. His results show that higher span numbers result in an increase of both the dynamic magnification displacement factor and the critical velocity. Therefore, the critical velocity is a crucial characteristic of beams.

A Bernoulli–Euler beam is the model generally employed in studying the problem of a beam subjected to moving loads. The wave velocity solution in the beam becomes unreasonable within the high frequency range [6]. This phenomenon means that the theory leads to erroneous results when a beam is subjected to a fast travelling load. Therefore, the effects of rotary inertia and shear deformation of the beam need to be considered. The resulting modified theory is called the Timoshenko beam theory [7]. The problem of a load travelling on a simply supported beam has been studied by Mackertich [8]. His results show that the deflection at the middle of the Timoshenko beam is greater than that of the Bernoulli–Euler beam.

In the aforementioned works, the effects of shear deformation and rotatory inertia on both the dynamic response and the critical velocity of a multi-span Timoshenko beam were

0022–460X/97/450731 + 12 $25.00/0/sv971188

rarely discussed. The deflection and its corresponding critical velocity will therefore be investigated in this paper. A uniform Timoshenko beam on regular supports is used as the model for study. Each span is isotropic and homogeneous. A concentrated force travelling at a constant velocity on the beam is presented as an example problem.

The finite element theory can be adopted as a technique for solving the problem of moving loads. However, the extensive computational time and memory storage requirements make the finite element technique impractical. Hence, we turn to the method of modal analysis as the most convenient alternative tool for studying beam vibration. We will investigate the suitability of modal analysis methodology for analyzing the vibration of a multi-span beam. Both the analytical method and the transfer-matrix method are employed to determine the modal frequencies and their corresponding mode shape functions of the multi-span beam. The orthogonality of the mode shape functions will be shown in order to guarantee the suitability of the method of modal analysis. The governing equation of each modal amplitude will be derived. The responses of the multi-span beam to a concentrated moving load is then presented as an example accompanied with a discussion of the differences in maximum moment, maximum deflection and critical velocity between the Timoshenko beam and the Bernoulli–Euler beam.

2. EQUATIONS OF MOTION

A multi-span Timoshenko beam subjected to a distributed load $\bar{F}(\bar{x}, \bar{t})$ is depicted in Figure 1. Each span of the beam is considered to be uniform and homogeneous. The non-dimensional forms of equations of motion of a typical span are

$$-\frac{\varepsilon}{r^2}\frac{\partial q}{\partial x} + \frac{\partial^1 w}{\partial t^2} = F(x, t), \qquad -\frac{\varepsilon q}{r^2} - \frac{\partial m}{\partial x} + r^2\frac{\partial^2 \psi}{\partial t^2} = 0, \tag{1a, b}$$

where

$$w = \bar{w}/h, \qquad x = \bar{x}/L, \qquad t = (EI/\rho AL^4)^{1/2}\,\bar{t}, \qquad \psi = \bar{\psi}L/h, \qquad m\,(=\partial\psi/\partial x) = \bar{m}L^2/EIh,$$

$$\varepsilon = \kappa G/E, \qquad r = \eta/L, \qquad q\,(=\partial w/\partial x - \psi) = \bar{q}L/\kappa GAh, \qquad F(x, t) = \bar{F}(\bar{x}, \bar{t})L^4/EIh,$$

in which E is Young's modulus, G is the shear modulus, κ is the shear coefficient, I is the second moment of the cross-section with respect to the neutral axis, L is the span length, h is the beam thickness, η is the radius of gyration of the cross-section, $\bar{m}$ is the bending moment, $\bar{q}$ is the shear force, $\bar{w}$ is the transverse deflection, $\bar{\psi}$ is the rotatory angle, $\bar{t}$ is time, A is the cross-sectional area, ρ is the density and $\bar{x}$ is the co-ordinate of the neutral axis.

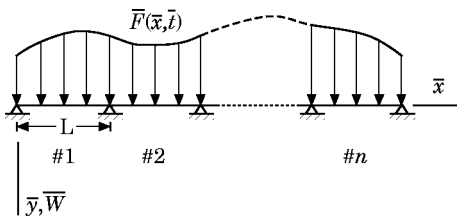

Figure 1. A multi-span Timoshenko beam subjected to a load $\bar{F}(\bar{x}, \bar{t})$.

3. FREE VIBRATION

For a steady state of free vibration, the transverse deflection, rotatory angle, shear force and moment of the jth span are denoted, respectively, as $w^{(j)}(\xi, t)$, $\psi^{(j)}(\xi, t)$, $q^{(j)}(\xi, t)$ and $m^{(j)}(\xi, t)$, which can be expressed as

$$\{w^{(j)} \quad \psi^{(j)} \quad q^{(j)} \quad m^{(j)}\}^{\mathrm{T}}(\xi, t) = \{W^{(j)} \quad \Psi^{(j)} \quad Q^{(j)} \quad M^{(j)}\}^{\mathrm{T}}(\xi)\, \mathrm{e}^{j\omega t}, \tag{2}$$

where ξ $(= x - j + 1)$ is the axial co-ordinate of the span and ω is the circular frequency. Combining equations (1a) and (1b) yields the equations of $W^{(j)}(\xi)$:

$$\frac{\mathrm{d}^4 W^{(j)}}{\mathrm{d}\xi^4} + r^2\omega^2\left(1 + \frac{1}{\varepsilon}\right)\frac{\mathrm{d}^2 W^{(j)}}{\mathrm{d}\xi^2} + \left(\frac{r^4\omega^4}{\varepsilon} - \omega^2\right)W^{(j)} = 0. \tag{3}$$

The zero transverse deflection at both ends of the span implies that the transverse deflection $W^{(j)}(\xi)$, rotatory angle $\Psi^{(j)}(\xi)$ and moment $M^{(j)}(\xi)$ are

$$W^{(j)}(\xi) = C_1^{(j)} D_1(\xi) + C_2^{(j)} D_2(\xi), \tag{4a}$$

$$\Psi^{(j)}(\xi) = C_1^{(j)} E_1(\xi) + C_2^{(j)} E_2(\xi), \tag{4b}$$

$$M^{(j)}(\xi) = C_1^{(j)} F_1(\xi) + C_2^{(j)} F_2(\xi), \tag{4c}$$

where $C_1^{(j)}$ and $C_2^{(j)}$ are two constants and the functions $D_1(\xi), \ldots$ and $F_2(\xi)$ are as listed in the Appendix.

Equations (4b) and (4c) are rearranged into the vector form as

$$\{\Psi^{(j)} \quad M^{(j)}\}^{\mathrm{T}}(\xi) = [R^{(j)}(\xi)]\{C_1^{(j)} \quad C_2^{(j)}\}^{\mathrm{T}} \tag{5}$$

from which $C_1^{(j)}$ and $C_2^{(j)}$ are solved in terms of the rotatory angle and moment at the left end of the span as

$$\{C_1^{(j)} \quad C_2^{(j)}\}^{\mathrm{T}} = [R^{(j)}(0)]^{-1}\{\Psi^{(j)} \quad M^{(j)}\}^{\mathrm{T}}(0). \tag{6}$$

The rotatory angle and moment become

$$\{\Psi^{(j)} \quad M^{(j)}\}^{\mathrm{T}}(\xi) = [N^{(j)}(\xi)]\{\Psi^{(j)} \quad M^{(j)}\}^{\mathrm{T}}(0), \tag{7}$$

where $[N^{(j)}(\xi)] = [R^{(j)}(\xi)]\,[R^{(j)}(0)]^{-1}$. Therefore, the relation of rotatory angle and moment at both ends of the span is

$$\{\Psi^{(j)} \quad M^{(j)}\}^{\mathrm{T}}(1) = [N^{(j)}(1)]\{\Psi^{(j)} \quad M^{(j)}\}^{\mathrm{T}}(0). \tag{8a}$$

The continuity of the rotatory angle and the balance of moment at the junction between two adjacent spans implies that equation (8a) will be of the form

$$\{\Psi^{(j+1)} \quad M^{(j+1)}\}^{\mathrm{T}}(0) = [N^{(j)}(1)]\{\Psi^{(j)} \quad M^{(j)}\}^{\mathrm{T}}(0), \tag{8b}$$

in which $[N^{(j)}(1)]$ is the transfer matrix.

The modal frequencies and their corresponding mode shape functions for the multi-span Timoshenko beam can be obtained by performing calculations similar to those described by Wang [9]. The ith modal frequency and the corresponding set of mode shape functions of the entire beam are denoted as ω_i and $\{W_i \;\; \Psi_i\}^{\mathrm{T}}(x)$, respectively.

4. ORTHOGONALITY

The ith modal frequency ω_i and the corresponding set of mode shape function W_i and Ψ_i satisfy the relations

$$\omega_i^2 W_i = -\frac{\varepsilon}{r^2}\frac{\mathrm{d}Q_i}{\mathrm{d}x}, \qquad r^2\omega_i^2 \Psi_i = -\frac{\varepsilon Q_i}{r^2} - \frac{\mathrm{d}M_i}{\mathrm{d}x}, \tag{9a, b}$$

where Q_i and M_i are the corresponding shearing force and moment respectively. Multiplying equation (9a) by W_j and equation (9b) by Ψ_j and integrating their sum from $x = 0$ to $x = n$ yields

$$\omega_i^2 \int_0^n (r^2 \Psi_i \Psi_j + W_i W_j)\,\mathrm{d}x = \frac{\varepsilon}{r^2}\int_0^n Q_i Q_j\,\mathrm{d}x + \int_0^n M_i M_j\,\mathrm{d}x. \tag{10}$$

Similarly, the following relation is obtained:

$$\omega_j^2 \int_0^n (r^2 \Psi_i \Psi_j + W_i W_j)\,\mathrm{d}x = \frac{\epsilon}{r^2}\int_0^n Q_i Q_j\,\mathrm{d}x + \int_0^n M_i M_j\,\mathrm{d}x. \tag{11}$$

Subtracting equation (11) from equation (10) yields

$$(\omega_i^2 - \omega_j^2)\int_0^n (r^2 \Psi_i \Psi_j + W_i W_j)\,\mathrm{d}x = 0, \qquad i \neq j, \tag{12}$$

which shows that any two distinct sets of the mode shape functions are orthogonal.

5. FORCED VIBRATION

According to the orthogonality of two distinct sets of the mode shape functions, the superposition method is adopted in the section to study the forced vibration of the multi-span beam. The respective transverse deflection, rotatory angle and the external load are expressed as

$$(w, \psi)(x, t) = \sum_{l=1} A_l(t)\,(W_l(x), \Psi_l(x)). \tag{13}$$

Substituting equation (13) into equations (1a) and (1b) yields

$$\sum_{l=1}\left(W_l\frac{\mathrm{d}^2 A_l}{\mathrm{d}t^2} - \frac{\varepsilon A_l}{r^2}\frac{\mathrm{d}Q_l}{\mathrm{d}x}\right) = F(x, t), \tag{14a}$$

$$\sum_{l=1}\left\{r^2\Psi_l\frac{\mathrm{d}^2 A_l}{\mathrm{d}t^2} - \left(\frac{\varepsilon Q_l}{r^2} + \frac{\mathrm{d}M_l}{\mathrm{d}x}\right)A_l\right\} = 0. \tag{14b}$$

Multiplying equation (14a) by $W_i(x)$ and equation (14b) by $\Psi_i(x)$ and performing their summation yields the governing equation of the ith modal amplitude as

$$\ddot{A}_i + \omega_i^2 A_i = f_i(t), \tag{15}$$

in which the dot represents differentiation with respect to time and the ith modal excitation $f_i(t)$ is

$$f_i(t) = \int_0^n F(x, t) W_i(x)\,\mathrm{d}x \Big/ \int_0^n (W_i^2 + r^2\Psi_i^2)\,\mathrm{d}x. \tag{16}$$

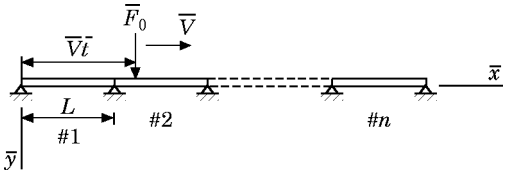

Figure 2. A moving load $\bar{F}_0$ on a multi-span beam.

6. MOVING FORCE

A concentrated force of magnitude $\bar{F}_0$ moving on the multi-span beam at a constant velocity $\bar{V}$ is depicted in Figure 2. Introducing the relevant variables,

$$V = \bar{V}(\rho A L^4/EI)^{1/2}/L, \qquad T = 1/V, \qquad F_0 = \bar{F}_0 L^3/EIh,$$

the non-dimensional form of the force is

$$F(x, t) = F_0 \delta(x - Vt), \qquad 0 \leqslant t \leqslant nT, \tag{17}$$

in which δ is the impulse function and T is the duration of time when the force travels on one span. The histories of the ith modal excitation $f_i(t)$, modal amplitude $A_i(t)$ and its corresponding velocity $\dot{A}_i(t)$, respectively, are:

(1) $0 \leqslant t \leqslant nT$,

$$f_i(t) = F_0 W_i(Vt) \Big/ \int_0^n (W_i^2 + r^2 \Psi_i^2)\, \mathrm{d}x, \tag{18a}$$

$$A_i(t) = A_i(0) \cos(\omega_i t) + \frac{\sin(\omega_i t)}{\omega_i} \dot{A}_i(0) + \frac{1}{\omega_i} \int_0^t f_i(t - \tau) \sin(\omega_i \tau)\, \mathrm{d}\tau, \tag{18b}$$

$$\dot{A}_i(t) - \omega_i A_i(0) \sin(\omega_i t) + \dot{A}_i(0) \cos(\omega_i t) + \int_0^t f_i(t - \tau) \cos(\omega_i \tau)\, \mathrm{d}\tau; \tag{18c}$$

(2) $nT < t$,

$$f_i(t) = 0, \tag{19a}$$

$$A_i(t) = A_i(nT) \cos(\omega_i t^*) + \frac{\sin(\omega_i t^*)}{\omega_i} \dot{A}_i(nT), \tag{19b}$$

$$\dot{A}_i(t) = -\omega_i A_i(nT) \sin(\omega_i t^*) + \dot{A}_i(nT) \cos(\omega_i t^*), \tag{19c}$$

in which $t^* = t - nT$.

7. EXAMPLES AND DISCUSSION

Each span of a multi-span beam with the same value of r is considered in the section. The data $\mu = 0{\cdot}3$, $\kappa = 0{\cdot}85$ and $F_0 = 1$ are taken for the purpose of numerical analysis. The value of the first modal frequency of the multi-span beam is independent of the span number. The effect of r on the frequency of the beam has been plotted in Figure 3 to show the proportionality of r to frequency. The frequency value of the Bernoulli–Euler beam is always greater than that of the Timoshenko beam, and this frequency deviation between the two beams will grow as the value of r increases. The result indicates that the Bernoulli–Euler beam is stiffer than the Timoshenko beam.

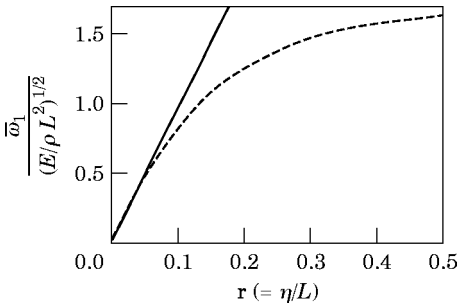

Figure 3. The r effect on the first modal frequency of a multi-span beam. ——, Bernoulli–Euler beam; ----, Timoshenko beam.

The initial conditions of the beam are set at zero. Results obtained by the modal analysis method converge rather fast. Therefore, it is sufficient to employ the lowest ten modal frequencies and their corresponding sets of mode shape functions of the entire beam in the method of modal analysis in the numerical computation. The following parameter definitions illustrate the numerical results: maximum deflection during the motion of the load, W_{max} ; maximum moment during the motion of the load, M_{max} ; position of maximum deflection during the motion of the load, X_W ; position of maximum moment during the motion of the load, X_M ; and velocity ratio, α ($= \bar{V}(\rho/E)^{1/2}$). The velocity range considered in this section is $0 < \alpha \leqslant 0{\cdot}25$.

The W_{max}–α distribution of a three-span beam ($r = 0{\cdot}05$) is shown in Figure 4(a). The critical velocity ratio α_c of displacement is governed by the first modal frequency of the beam. The value of the first modal frequency of the Timoshenko beam is less than that of the Euler beam. Therefore, the critical velocity of the Timoshenko beam is less than that of the Bernoulli–Euler beam as shown in Figure 4(a). Within the subcritical velocity range $0 \leqslant \alpha \leqslant \alpha_c$, the effects of shear deformation and bending moment always force W_{max} of the Timoshenko beam to be greater than that of the Bernoulli–Euler beam due to bending moment only. The effects of rotatory inertia and shear deformation cause the modal frequencies of the Timoshenko beam to be less than those of the Bernoulli–Euler

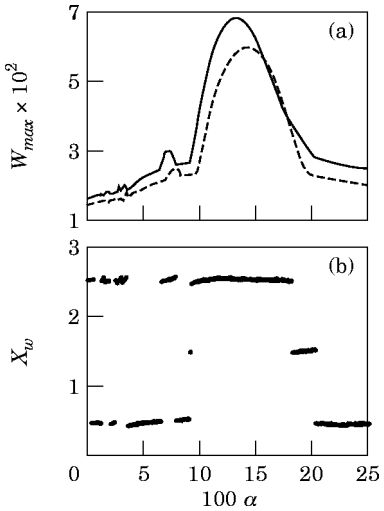

Figure 4. The W_{max}–α distribution (a) and its corresponding X_w–α distribution (b) of a three-span Timoshenko beam ($r = 0{\cdot}05$). ——, Timoshenko beam; ----, Bernoulli–Euler beam.

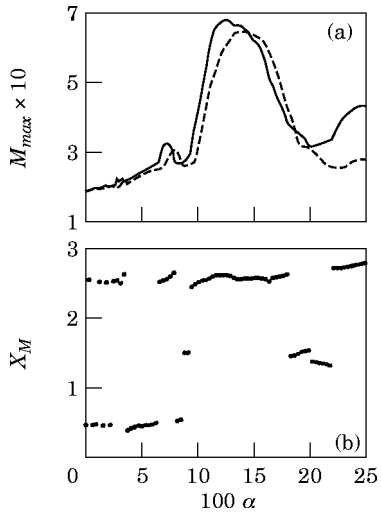

Figure 5. The M_{max}–α distribution (a) and its corresponding X_M–α distribution (b) of a three-span Timoshenko beam ($r = 0{\cdot}05$). ——, Timoshenko beam; ----, Bernoulli–Euler beam.

beam. Furthermore, the deviation of a modal frequency between these two beams increases as the mode number increases. This result indicates that the Bernoulli–Euler beam is stiffer than the Timoshenko beam. A rapidly moving force will excite the response of the higher modes. As a result, the W_{max} of the Timoshenko beam is greater than that of the Bernoulli–Euler beam within the supercritical velocity range. The moments at the simply supports of the beam are zero. As a result, the X_W–α distribution of the Timoshenko beam displayed in Figure 4(b) indicates that the maximum deflection always occurs in close proximity to the mid-point of one span.

The M_{max}–α distribution of the three-span beam ($r = 0{\cdot}05$) is shown in Figure 5(a). The bending effect is the governing factor on the moment distribution of a beam to a static force. The moving force can be regarded as a quasi-static force at the low velocity ratio. This figure therefore reveals that the M_{max} of the Timoshenko beam is almost the same as that of the Bernoulli–Euler beam within the velocity range $0 \leqslant \alpha \leqslant 0{\cdot}05$. However, the M_{max} difference between the two beams becomes apparent within the velocity range $0{\cdot}1 \leqslant \alpha \leqslant \alpha_c$. The absolute M_{max} of the Timoshenko beam is greater than that of the Bernoulli–Euler beam. The effects of rotatory inertia and shear deformation cause the M_{max} of the Timoshenko beam to be greater than that of the Bernoulli–Euler beam within the supercritical velocity range $0{\cdot}2 \leqslant \alpha \leqslant 0{\cdot}25$. The X_M–α distribution of the Timoshenko beam displayed in Figure 5(b) indicates that the maximum moment almost occurs near the mid-point of one span.

The comparisons of the three different α effects on the history of the deflection at the three-quarters length of the third span of a three-span Timoshenko beam ($r = 0{\cdot}05$) are displayed in Figures 6(a)–6(c). A faster speed of the moving force results in a shorter duration of forced vibration of the beam. As a result, Figure 6(a) reveals that a large deflection appears when the force travels on the beam at the velocity ratio $\alpha = 0{\cdot}047$. Moreover, in Figure 6(b) it is shown that maximum deflection occurs as the force is leaving the beam at the critical velocity ratio. A large deflection induced by a supercritical moving force ($\alpha = 0{\cdot}173$) will appear after the load has left the beam, as indicated in Figure 6(c). The three corresponding moment histories are displayed in Figures 7(a)–7(c). The times

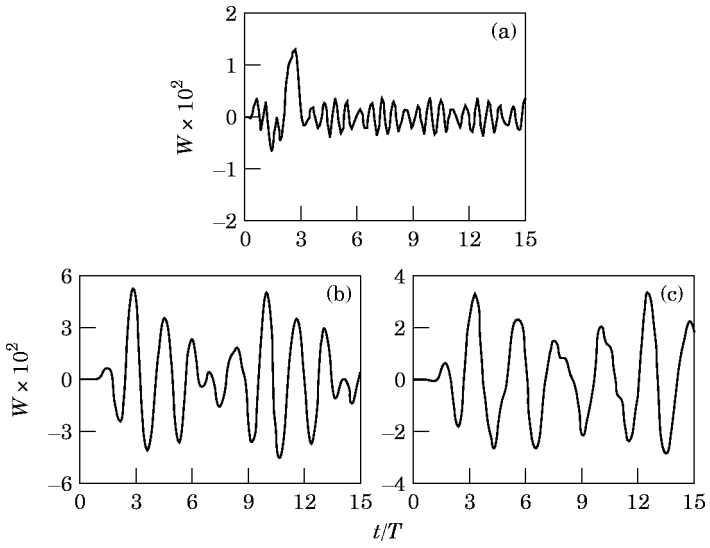

Figure 6. Comparisons of three different α effects on the deflection history of the mid-point of the last span of a three-span Timoshenko beam ($r = 0{\cdot}05$): (a) $\alpha = 0{\cdot}047$; (b) $\alpha = \alpha_c$; (c) $\alpha = 0{\cdot}173$.

at which the maximum moment in these three figures occur are very similar to those in Figures 6(a)–6(c).

The effects of the span number on the W_{max}–α distribution and the M_{max}–α distribution of the multi-span Timoshenko beam ($r = 0{\cdot}05$) are displayed in Figures 8(a) and 8(b) respectively. Both the total length and the weight of the Timoshenko beam increase as the span number increases. The moving force is regarded as a quasi-static load within the low velocity range $0 \leqslant \alpha \leqslant 0{\cdot}05$. The higher span number results in a heavier mass of the entire beam. As a result, in Figures 8(a) and 8(b) it is shown that the higher the number of the span, the lower both W_{max} and M_{max} are within the velocity range. A force travelling on

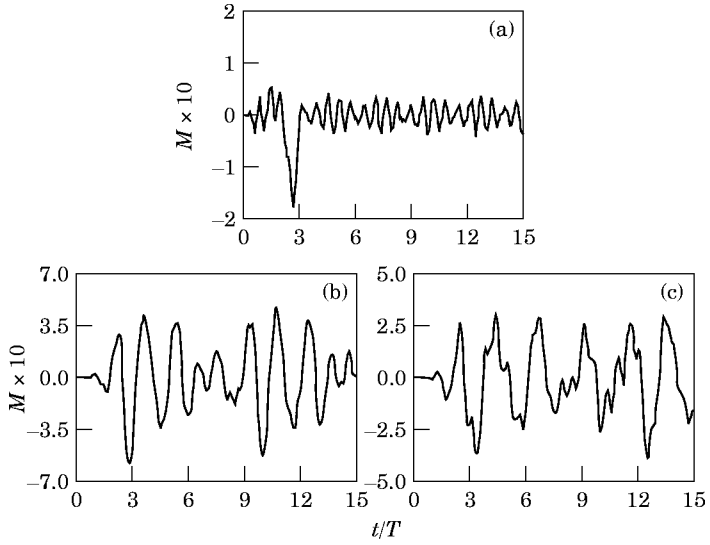

Figure 7. Comparisons of three different α effects on the moment history of the mid-point of the last span of a three-span Timoshenko beam ($r = 0{\cdot}05$): (a) $\alpha = 0{\cdot}047$; (b) $\alpha = \alpha_c$; (c) $\alpha = 0{\cdot}173$.

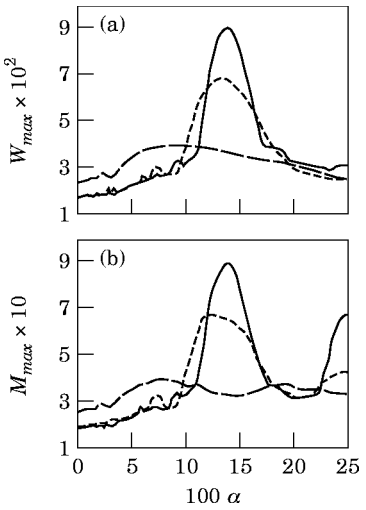

Figure 8. The span number effect on (a) the W_{max}–α distribution and (b) the M_{max}–α distribution of a multi-span Timoshenko beam ($r = 0{\cdot}05$). ——, Five spans; ----, three spans; ——, one span.

the beam induces a disturbance propagation in the beam. The composition of the disturbance includes free waves and non-propagating parts, which attenuate spatially. Consequently, the effect of free waves on the vibration of the beam is more apparent for higher span numbers. The vibration of the beam is dominated by the first modal frequency of the structure. The first mode shape of the beam is a bending mode. Both figures therefore demonstrate that the higher the number of the span, the more both W_{max} and M_{max} are constrained within the neighborhood of the critical velocity of a bending wave. In Table 1 it is shown that the critical velocity will approach the lowest bending wave phase velocity in the beam as the span number increases. In Table 2 it is shown that the larger the span number is, the greater is the value of the maximum deflection. Mead [10] has found that an infinite regularly supported beam, which is subjected to a force travelling with a bending wave phase velocity, will deform seriously. The results presented in Tables 1 and 2 agree with Mead's prediction.

TABLE 1

The effect of span number on the critical velocity ratio $100\alpha_c$ *of a multi-span beam* ($r = 0{\cdot}05$)

Span	Bernoulli–Euler beam	Timoshenko beam
1	9·896	9·111
2	13·823	12·566
3	14·137	13·195
4	14·294	13·509
5	14·294	13·666
6	14·294	13·823
*	15·708	14·988

* The lowest phase velocity ratio of bending wave in the beam.

TABLE 2

The effect of span number on the absolute maximum deflection ($100W_{max}$) *of a multi-span beam* ($r = 0{\cdot}05$)

Span	Bernoulli–Euler beam	Timoshenko beam
1	3·623	3·911
2	4·860	5·365
3	5·967	6·825
4	6·773	8·049
5	7·502	9·054
6	8·357	9·861

8. CONCLUSIONS

The value of the first modal frequency of a multi-span beam is independent of the span number. The effects of rotatory inertia and of shear deformation on lowering the first modal frequency are apparent for a beam with a high ratio of radius of gyration to span length. Within the neighborhood of the critical velocity, the effects of rotatory inertia and shear deformation cause greater absolute maximum deflection than the bending effect alone. Both a large deflection and a large moment of a beam induced by a force moving with a subcritical velocity occur while the force travels on the beam. Moreover, a force moving with the critical velocity causes both the maximum deflection and the maximum moment of a beam to appear while the force is leaving the beam. Higher span numbers result in higher absolute maximum deflection, absolute maximum moment and critical velocity. The upper bound of the critical velocity is the lowest phase velocity of the bending wave in the beam.

ACKNOWLEDGMENT

This work was sponsored by the National Science Council, ROC, under Contract No. 84-221-E006-085. The financial support is greatly acknowledged.

REFERENCES

1. L. FRY'BA 1971 *Vibration of Solids and Structures under Moving Loads*. Groningen: Noordhoff International.
2. T. E. BLEJWAS, C. C. FENG and R. S. AYRE 1979 *Journal of Sound and Vibration* **67**, 513–521. Dynamic interaction of moving vehicles and structures.
3. M. OLSSON 1991 *Journal of Sound and Vibration* **145**, 299–307. On the fundamental moving load problem.
4. J. GENIN and Y. I. CHUNG 1979 *Journal of Sound and Vibration* **67**, 245–251. Response of a continuous guideway on equally spaced supports traversed by a moving vehicle.
5. R. T. WANG 1994 *Journal of the Chinese Society of Mechanical Engineers* **15**(3), 229–235. Vibration analysis of multispan beams subjected to moving loads using the finite element method.
6. H. KOLSKY 1963 *Stress Waves in Solids*. New York: Dover.
7. S. P. TIMOSHENKO and D. H. YOUNG 1974 *Vibration Problems in Engineering*. New York: John Wiley.
8. S. MACKERTICH 1990 *Journal of Acoustical Society of America* **88**(2), 1175–1178. Moving load on a Timoshenko beam.
9. R. T. WANG 1993 *Journal of the Chinese Society of Mechanical Engineers* **14**(6), 599–604. Comparative study on free vibration of multispan beams between analytic solution and finite element-transfer matrix computation.

10. D. J. MEAD 1986 *Journal of Sound and Vibration* **104**, 9–27. A new method of analyzing wave propagation in periodic structures applications to periodic Timoshenko beams and stiffened plates.

APPENDIX: LIST OF FUNCTIONS $D_1(\xi)$, $D_2(\xi)$, ETC.

(1) For $\omega^2 < \varepsilon/r^4$:

$$D_1(\xi) = \cos(\lambda_1\xi) - \cosh(\lambda_2\xi) - [\cos(\lambda_1) - \cosh(\lambda_2)]\sinh(\lambda_2\xi)/\sinh(\lambda_2),$$

$$D_2(\xi) = \sin(\lambda_1\xi) - \sin(\lambda_1)\sinh(\lambda_2\xi)/\sinh(\lambda_2),$$

$$E_1(\xi) = \left(\frac{\omega^2}{\lambda_1\varepsilon r} - \lambda_1\right)\sin(\lambda_1\xi) - \left(\frac{\omega^2}{\lambda_2\varepsilon r} + \lambda_2\right) \times \left\{\sinh(\lambda_2\xi) + \frac{[\cos(\lambda_1) - \cosh(\lambda_2)]\cosh(\lambda_2\xi)}{\sinh(\lambda_2)}\right\},$$

$$E_2(\xi) = -\left(\frac{\omega^2}{\lambda_1\varepsilon r} - \lambda_1\right)\cos(\lambda_1\xi) - \left(\frac{\omega^2}{\lambda_2\varepsilon r} + \lambda_2\right)\sin(\lambda_1)\cosh(\lambda_2\xi)/\sinh(\lambda_2),$$

$$F_1(\xi) = \left(\frac{\omega^2}{\varepsilon r} - \lambda_1^2\right)\cos(\lambda_1\xi) - \left(\frac{\omega^2}{\varepsilon r} + \lambda_2^2\right)\left\{\cosh(\lambda_2\xi) + \frac{[\cos(\lambda_1) - \cosh(\lambda_2)]\sinh(\lambda_2\xi)}{\sinh(\lambda_2)}\right\},$$

$$F_2(\xi) = -\left(\frac{\omega^2}{\varepsilon r} - \lambda_1^2\right)\sin(\lambda_1\xi) - \left(\frac{\omega^2}{\varepsilon r} + \lambda_2^2\right)\sin(\lambda_1)\sinh(\lambda_2\xi)/\sinh(\lambda_2), \quad \text{(A1)–(A6)}$$

where

$$\lambda_1^2 = \frac{\omega^2 r^2(1+\varepsilon)}{2\varepsilon} + \sqrt{\frac{r^4\omega^4}{4\varepsilon^2}(1-\varepsilon)^2 + \omega^2},$$

$$\lambda_2^2 = -\frac{\omega^2 r^2(1+\varepsilon)}{2\varepsilon} + \sqrt{\frac{r^4\omega^4}{4\varepsilon^2}(1-\varepsilon)^2 + \omega^2}.$$

(2) For $\omega^2 > \varepsilon/r^4$:

$$D_1(\xi) = \cos(\lambda_1\xi) - \cos(\lambda_2\xi) - [\cos(\lambda_1) - \cos(\lambda_2)]\sin(\lambda_2\xi)/\sin(\lambda_2),$$

$$D_2(\xi) = \sin(\lambda_1\xi) - \sin(\lambda_1)\sin(\lambda_2\xi)/\sin(\xi_2),$$

$$E_1(\xi) = \left(\frac{\omega^2}{\lambda_1\varepsilon r} - \lambda_1\right)\sin(\lambda_1\xi) + \left(\frac{\omega^2}{\lambda_2\varepsilon r} - \lambda_2\right) \times \left\{-\sin(\lambda_2\xi) + \frac{[\cos(\lambda_1) - \cos(\lambda_2)]\cos(\lambda_2\xi)}{\sin(\lambda_2)}\right\},$$

$$E_2(\xi) = -\left(\frac{\omega^2}{\lambda_1 \varepsilon r} - \lambda_1\right)\cos(\lambda_1 \xi) + \left(\frac{\omega^2}{\lambda_2 \varepsilon r} - \lambda_2\right)\sin(\lambda_1)\cos(\lambda_2 \xi)/\sin(\lambda_2),$$

$$F_1(\xi) = \left(\frac{\omega^2}{\varepsilon r} - \lambda_1^2\right)\cos(\lambda_1 \xi) + \left(\frac{\omega^2}{\varepsilon r} - \lambda_2^2\right)\left\{-\cos(\lambda_2 \xi) - \frac{[\cos(\lambda_1) - \cos(\lambda_2)]\sin(\lambda_2 \xi)}{\sin(\lambda_2)}\right\},$$

$$F_2(\xi) = \left(\frac{\omega^2}{\varepsilon r} - \lambda_1^2\right)\sin(\lambda_1 \xi) - \left(\frac{\omega^2}{\varepsilon r} - \lambda_2^2\right)\sin(\lambda_1)\sin(\lambda_2 \xi)/\sin(\lambda_2), \quad \text{(A7)–(A12)}$$

where

$$\lambda_1^2 = \frac{\omega^2 r^2(1+\varepsilon)}{2\varepsilon} + \sqrt{\frac{r^4\omega^4}{4\varepsilon^2}(1-\varepsilon)^2 + \omega^2},$$

$$\lambda_2^2 = \frac{\omega^2 r^2(1+\varepsilon)}{2\varepsilon} - \sqrt{\frac{r^4\omega^4}{4\varepsilon^2}(1-\varepsilon)^2 + \omega^2}.$$